Top Catal (2016) 59:241–251
DOI 10.1007/s11244-015-0437-2

ORIGINAL PAPER

Deep Hydrodesulfurization of Dibenzothiophenes Over NiW Sulfide Catalysts Supported on Sol–Gel Titania–Alumina

J. A. Tavizón-Pozos[1] · V. A. Suárez-Toriello[1] · J. A. de los Reyes[1] · A. Guevara-Lara[2] · B. Pawelec[3] · J. L. G. Fierro[3] · M. Vrinat[4] · C. Geantet[4]

Published online: 11 August 2015

Abstract This work showed that the use of Al_2O_3–TiO_2 as carriers has a positive effect on the activity of supported NiW catalysts in the hydrodesulfurization of dibenzothiophene and 4,6-dimethyldibenzothiophene carried out in a batch reactor at 320 °C and total H_2 pressure of 5.5 MPa. Two Al_2O_3–TiO_2 mixed oxides with Al/Ti atomic ratios of 10 and 2 were synthesized by sol–gel method together with the pure Al_2O_3 synthesized as reference support. For NiW/Al_2O_3–TiO_2 and NiW/Al_2O_3 catalysts, a metal load of 17 and 5.5 wt% of W and Ni were considered respectively. It was found that both Al_2O_3–TiO_2-supported catalysts exhibited higher activity than alumina-supported one. The catalyst with a largest TiO_2 content (NiW/AT2) demonstrated to be 23 % more active with respect to NiW/Al_2O_3. Solids were characterized by temperature-programmed reduction (TPR), high resolution transmission electronic microscopy and X-ray photoelectronic spectroscopy (XPS) techniques. A decrease in support–metal interaction (from TPR) was observed when Ti content increased, which could lead to a higher amount of NiWS phase (from XPS). Besides, a slight increase in the slabs length in WS_2 was observed for titania-containing catalyst with respect to NiW/Al_2O_3, indicating that the dispersion can still be optimized. The atomic ratio Al/Ti = 2 of the NiW/Al_2O_3–TiO_2 catalyst proved to be a potential substitute for current catalysts for sulfur reduction in ultra-clean diesel.

Keywords Hydrodesulfurization · NiW · Dibenzothiophene · 4,6-Dimethyldibenzothiophene · Al_2O_3–TiO_2 mixed oxide · Support–metal interaction

✉ J. A. de los Reyes
jarh@xanum.uam.mx

1 Área de Ingeniería Química, Universidad A. Metropolitana-Iztapalapa, Av. FFCC R. Atlixco 186, 09340 Mexico, Distrito Federal, Mexico

2 Centro de Investigaciones Químicas, Universidad Autónoma del Estado de Hidalgo, Ciudad Universitaria, 42184 Pachuca, Mexico

3 Instituto de Catálisis y Petroleoquímica, CSIC, C/Marie Curie 2, Cantoblanco, 28049 Madrid, Spain

4 Institut de Recherches sur la Catalyse et l'Environnement de Lyon, UMR 5256 CNRS-Université Lyon 1, 2 Av. Einstein, 69626 Villeurbanne Cedex, France

1 Introduction

The severe environmental restrictions on the amount of sulfur in diesel have made necessary to improve the catalysts used in hydrodesulfurization (HDS). This, because the refractory sulfur compounds such as dibenzothiophene (DBT) and 4,6-dimethyldibenzothiophene (4,6-DMDBT), which exhibit steric hindrance by the alkyl groups on their molecular structure, are present in the oil cuts. Thus, these compounds display a route to hydrogenation in the HDS reaction [1]. In contrast to hydrotreating (HDT) common catalysts, NiMo and CoMo supported on Al_2O_3, the NiW/Al_2O_3 catalysts and their outstanding hydrogenating properties exhibit, therefore, potential for deep HDS [2, 3]. However, this catalyst shows incomplete sulfidation and migration of Ni species into the alumina structure. Also there is segregation of NiS_x species and lack of promotion for the NiWS phase is obtained. This mixed phase is responsible for the activity in these systems [4–7]. In particular, the formation of strong W–O–Al bonds prevents sulfidation of the W phase, while the high affinity between the Ni^{2+} ions and surface vacancies Al^{3+} on the support limits the availability of the Ni, on its deposition on the edges of WS_2 crystallites [8]. To avoid this problem, NiW

has been tested on TiO_2 support, showing promising results [9, 10]. Nevertheless, it has been discarded for industrial purposes because low specific areas (10–150 m^2 g^{-1}) and low thermal stability for TiO_2. Consequently, the modification and development of new supports has been used as a strategy to modify the surface properties, to optimize the formation of the active phase and to improve the catalytic performance [11].

In order to improve these two supports, it has been proposed to use the binary system of Al_2O_3–TiO_2, because it has shown higher catalytic activity than alumina [12–14]. It has been reported that the presence of TiO_2 in the support facilitated the reduction and sulfidation for Ni–W phases, and decreased interactions between W oxide precursors with the support. Also, the presence of the Ti induced more WS_2 species than on alumina, favoring the hydrogenation route in the HDS of probe molecules, which requires hydrogenation of one of its aromatic rings before hydrodesulfurization [15–20].

In these systems, the synthesis method and composition are important aspects to control the interaction between the active phase and the support [16, 21]. A significant increase in HDS activity was found for the NiW/Al_2O_3–TiO_2 catalysts prepared by coprecipitation or supported on alumina impregnated with titania [9, 22, 23]. It has been proposed that TiO_2 would transfer electrons to the active phase helping NiWS sulfide reducibility with the formation of sulfur vacancies [24]. Duan et al. [20] found that for NiW/Al_2O_3–TiO_2, synthetized by sol–gel method had higher activity than NiW/Al_2O_3 in the HDS of diesel oil. They found that the optimal TiO_2 content was around 15 wt%. Also, some of us [25] reported that the impregnation pH of the active phase is important to these systems. At high pH impregnation solutions the Ni–W interactions would be higher than at low pH impregnation solutions because the relation between the W solution species formed and the support point zero charge (PZC).

The use of the sol–gel method may allow the synthesis of mixed oxides of Al_2O_3–TiO_2, in this system interactions between the active phase and the support might be substantially different from those published previously [19, 26]. In addition to improving the textural properties, these materials exhibited particular structural configuration that may result in synergistic effects or a combination of surface properties of both oxides [27]. Thus, this system would allow modulating support–metal interactions, which might benefit the efficiency of the NiW catalytic systems. In addition, it is necessary to shed light on issues such as the NiWS phase formation or if the WO_X entities are entirely sulfided, i.e., the genesis of sulfides phases. Consequently, this paper focuses on NiW catalysts supported on titania-alumina synthesized by the sol–gel method, with the aim to understand more deeply the genesis of the NiWS active phase and its relationship with catalytic performance. For this purpose, the catalysts were characterized by X-ray photoelectron spectroscopy (XPS), high resolution transmission electron microscopy (HRTEM), temperature-programmed reduction (TPR), temperature-programmed desorption of ammonia (TPD-NH_3), electrophoresis (Potential ζ) and nitrogen physisorption. Catalytic evaluation in HDS was carried out in model reactions using dibenzothiophene (DBT) or 4,6-dimethyldibenzothiophene (4,6-DMDBT).

2 Experimental

2.1 Synthesis of Materials

Various NiW/Al_2O_3–TiO_2 catalysts were prepared with different molar Al/Ti ratio in the support (Al/Ti = ∞, 10 and 2; see Table 1). Tungsten and nickel loadings in catalysts were 17 and 5.5 wt%, respectively (see Table 2). Low temperature sol–gel technique [26] with HNO_3 as hydrolysis catalyst and calcination at 400 °C for 5 h in static air atmosphere was used to prepare Al_2O_3 and the different Al_2O_3–TiO_2 mixed oxides. The structural conformation and textural properties of the supports were described previously by Nuñez et al. [28]. The supports were impregnated by successive incipient wetness technique; firstly tungsten was impregnated and then nickel was deposited. Aqueous solution of ammonium metatungstate hydrate $(NH_4)_6W_{12}O_{40}\cdot xH_2O$, and nickel nitrate hexahydrate, $Ni(NO_3)_2\cdot 6H_2O$, were used as precursors of

Table 2 Metal loading of the catalysts determined by ICP–OES

Sample	Ni (wt%)	W (wt%)
NiW/Al	5.3	15.3
NiW/AT10	6.0	16.6
NiW/AT2	4.7	18.6

Table 1 Textural properties of the synthetized supports

Support	Al/Ti atomic ratio	Nomenclature	S_{BET} (m^2 g^{-1})	V_p (cm^3 g^{-1})	d_p (nm)	PZC
Al_2O_3	∞	Al	259	0.95	9.5	8.5
Al_2O_3–TiO_2	10	AT10	343	1.0	7.9	8.2
Al_2O_3–TiO_2	2	AT2	359	1.1	7.7	7.6

W and Ni respectively. After each impregnation step, the catalysts were aged for 12 h at room temperature, and then dried at 120 °C for 12 h. The dried NiW catalysts were calcined at 400 °C for 5 h, and then stored in a moisture-free container for further characterization or sulfidation.

2.2 Materials Characterization

The BET surface area, pore volume, and pore size for the synthesized supports were measured with a Quantachrome Autosorb-1 instrument using N_2 adsorption–desorption isotherms at -192 °C. Before the measurement, the sample was degassed ($<10^{-2}$ Pa) at 350 °C. The surface area was obtained from the adsorption isotherm data ($0.1 < P/P_0 < 0.3$) using the multi-point Brunauer–Emmett–Teller (BET) method. The total pore volume was determined by N_2 adsorption at $P/P_0 = 0.99$. The pore size was obtained from desorption isotherm by the Barrett–Joyner–Halenda (BJH) method.

Determinations of the Zeta (ζ) potential were made with a Malvern Zetasizer 3000. For this, fine particles of support (50 mg) were dispersed in a 0.01 M solution of KOH at 25 °C. The pH value of the solutions was adjusted with aqueous solutions of NH_4OH or HNO_3 (0.01 M each). The metal loading of the oxide precursors was determined by inductively coupled plasma–atomic emission spectroscopy (ICP–AES), PerkinElmer Optima 3300 DV. For these analyses, the samples were previously digested in a mixture of HF, HCl and HNO_3 in a microwave oven for 2 h.

Temperature-programmed reduction (TPR) and temperature-programmed desorption of ammonia (TPD-NH_3) experiments were carried out with a Micromeritics TPR/TPD 2900 apparatus provided with a thermal conductivity detector (TCD) interfaced to a data station. For each TPR or TCD-NH_3 test, about 50 mg of sample were placed into a quartz cell (U-shaped) and pretreated in situ at 250 °C for 1 h under He flow to remove water and other contaminants. Additionally, a moisture trap was used to prevent TCD interference. After this, the samples were cooled to room temperature. TPR analysis was performed under a stream of 10 vol% of H_2/Ar, with a heating rate of 15 °C min^{-1} up to 1100 °C. For the TPD- NH_3 experiment, the samples were ammonia-saturated in a stream of 5 % NH_3/He (50 mL min^{-1}) at 100 °C for half an hour. Then, the physically adsorbed NH_3 was removed by a treatment in a He flow at 100 °C for 15 min. The ammonia desorption was performed under H_2 stream from 100 to 1000 °C using heating rate of 15 °C min^{-1}.

X-ray photoelectron spectroscopy (XPS) for both freshly sulfided and after reaction catalysts were carried out in a VG ESCALAB 200R spectrometer equipped with a hemispherical electron analyzer and a Mg Kα (hν = 1253.6 eV) X-ray source. The residual pressure was kept below 7×10^{-7} Pa during data acquisition. The binding energies (BE) were referenced to the C 1 s peak (284.9 eV) to account for the charging effects. The areas of the peaks were computed after fitting of the experimental spectra to Gaussian/Lorentzian curves and removal of the background (Shirley function). Surface atomic ratios were calculated from the peak area ratios normalized by the corresponding atomic sensitivity factors. For more details about XPS measurements one can see [29]. The high resolution transmission electron microscopy (HRTEM) was carried out in a JEM 2100F microscope operating with a 200 kV accelerating voltage and fitted with an INCA X-SIGHT (Oxford Instruments). In order to obtain statistically reliable information, the slab length of ca. 300 particles was measured for each freshly sulfide catalysts. Moreover, the particle size distribution was evaluated by counting in micrographs taken for the same sample. Prior to the XPS, HRTEM or catalytic activity experiments, the oxide NiW catalysts were sulfided with a mixture of 10 vol% H_2S/H_2 (4 L min^{-1}) at 400 °C for 4 h. A heating rate 5 °C min^{-1} was used. After this step, the sulfide catalysts were cooled to room temperature and flushed with N_2 for about half an hour. Immediately, the freshly sulfide NiW catalysts were immersed in isooctane to avoid air exposure. Subsequently, the samples were degassed (10^{-3} Pa) and immediately transferred without air exposure under argon atmosphere to XPS or HRTEM analysis. For catalytic activity, the freshly sulfided catalysts were directly immersed in the reaction mixture.

The coke deposited on the spent catalysts was quantified by thermogravimetry (Mettler Toledo TGA/SDTA851 equipment) by comparison of the TPO/TG profiles of spent catalysts with those of their fresh counterparts. Before TG/DTG measurements, the sample was dried in pure N_2 at 500 °C for 1 h in order to remove water and other contaminants from the catalyst surface. The TPO experiments were carried out by raising sample temperature from room temperature to a final temperature of 900 °C at a rate of 10 °C min^{-1} in a 20 vol% O_2/N_2 gas mixture (50 mL min^{-1}).

Raman spectra were obtained at room temperature on a T64000 triple monochromator Jobin–Yvon-Horiba using the 514.5 nm line of an Ar^+ laser (Lexel Laser). All the spectra were obtained at a power of 10 mW at the laser head, in the range 10–1600 cm^{-1}, and 1 cm^{-1} resolution. An Olympus microscope with a ×100 objective and 10 accumulations of 60 s each was used. Gaussian deconvolution of spectra was performed according to a previous report by Diaz de Leon et al. [30].

2.3 Catalytic Activity

Catalytic activities for sulfide catalysts were evaluated by the hydrodesulfurization of dibenzothiophene (DBT) and

4,6-dimethyldibenzothiophene (4,6-DMDBT). The reaction took place in a high-pressure batch reactor (Parr Instrument Co.) equipped with magnetic agitation, wall-baffles, gas inlet and outlet valves, a liquid sample valve, pressure gauge and internal thermocouple. The reaction mixture consisted in DBT or 4,6-DMDBT (300 ppm of sulfur) dissolved in 100 mL of solvent and 250 mg of freshly sulfide catalyst. In order to improve product quantification by chromatography analysis, different solvents were used: hexadecane for DBT and dodecane for 4,6-DMDBT. Once closed the reactor, the reaction system was flushed with N_2 to displace air. Then, reactor was pressurized at 1.4 MPa with N_2 and heated to the reaction temperature (320 °C). Subsequently, N_2 was vented slowly, and then H_2 was introduced up to reaction pressure (5.4 MPa). The reaction pressure was kept constant by manual addition of H_2. Reaction was carried out with vigorous agitation (1200 rpm). The reaction time was considered to star from the incorporation of H_2. Small samples volume were periodically collected (0, 15, 30, 45, 60, 90, 120, 150, 180 and 240 min; the sum was <5 % of initial volume) and analyzed by a gas chromatograph (PerkinElmer Autosystem XL) equipped with a HP-5 capillary column (5 % phenyl-methyl-silicone, 30 m × 0.25 mm) and a flame ionized detector (FID). The initial reaction rate ($(-r_A)'$; Ec. 1) expresses the catalytic activity (mol transformed of reactive per second and gram of sulfided catalyst, mol s^{-1} g^{-1}).

$$(-r_A)' = \left(\frac{dC_A}{dt}\right) \cdot w^{-1} \quad (1)$$

where (dC_A/dt) is the rate of change of the molar concentration of reagent (C_A) with respect to the time (t), and will be obtained by the initial constant slope of a plot of C_A versus t. w is the mass of freshly sulfided catalyst. After the reaction, the spent catalyst was filtered and stored in inert atmosphere.

3 Results and Discussion

3.1 Catalysts Characterization

3.1.1 Textural Properties

The textural properties and point of zero charge (PZC) for supports prepared by sol–gel technique are given in Table 1. The incorporation of Ti in Al_2O_3 produced around 30 % higher surface areas (S_{BET}) and 18 % lower pore diameter (d_p) compared with pure Al_2O_3. A significant variation in total pore volume (V_P) was not observed. However, the textural properties of these Al_2O_3–TiO_2 mixed oxides were suitable for potential implementation in diesel cuts hydrotreating [11]. In addition, a decrease in PZC values was observed as Al/Ti ratio was increased, suggesting that incorporation of Ti induced superficial modifications in the supports. Since PZC of support influences the support–metal interaction [31], special attention should be paid to the conditions of impregnation. In this sense, a maximum concentration of anions species of W ($HW_6O_{20}^{3-}$ and $HW_6O_{20}(OH)_2^{5-}$) and a majority of positive surface charges exist simultaneously at pH 4 [32, 33]. At these conditions, the W species may be properly anchored by electrostatic interactions.

3.1.2 Temperature-Programmed Reduction (TPR)

The TPR profiles for the supported NiW catalysts are shown in Fig. 1. In Fig. 1a can be observed that the alumina supported catalyst showed two reduction peaks at 625 and 905 °C. The peak at 625 °C is attributed to the Ni reduction as $NiWO_4$ and a partial reduction of the surface W ($W^{6+} \rightarrow W^{4+}$) [9, 34]. For AT2 this reduction step was identified at 603 °C. Also, the main peak could be associated with the overall reduction of bulk tungsten $W^{4+} \rightarrow W^0$. For the Al_2O_3–TiO_2-supported samples, the peaks were shifted toward lower temperatures, suggesting a decrease in the metal–support interaction related to the increasing amount of Ti. A similar effect was observed for the sulfided catalysts depicted in Fig. 1b. The first peak at 233–256 °C has been attributed to physisorbed H_2S. The next region between 380 and 600 °C has been related to the presence of Ni sulfided species such as NiS and NiWS. The last wide region (>600 °C) could be attributed to the combination of bulk WS_2 and partially oxide species [3, 35, 36]. It is possible to assume that a significant amount of Ni was present as NiWS and $NiWO_4$ phases. Considering that it has been indicated that $NiWO_4$ over alumina is not completely sulfided at 400 °C [3, 36], it could be said that a higher amount of Ni and W species were in the NiWS phase over the alumina-titania support since the reduction is presented at lower temperatures. However, it has been mentioned that the NiWS phase segregation resulting in the formation of Ni_3S_2 and WS_2. Thus, the amount of NiWS decreases [35–37]. This may indicate that the WS_2 reduction occurs in one step while the sulfided Ni is reduced in two steps (NiS → Ni_3S_2 → Ni) [3, 36, 37]. Since over the AT2 support the reduction of the metalic sulfide is presented at lower temperatures than in AT10 and alumina support, this could suggest that the modification of the Al_2O_3 support with TiO_2 decreases the support–metal interactions and the reduction of Ni and W sulfided species may be easier. Considering the amount of H_2 consumed (Fig. 1a), the observed trend is: NiW/AT2 > NiW/AT10 > NiW/Al. Since the catalyst initial activities (Fig. 5a, b) follows the same trend as the H_2 consumed

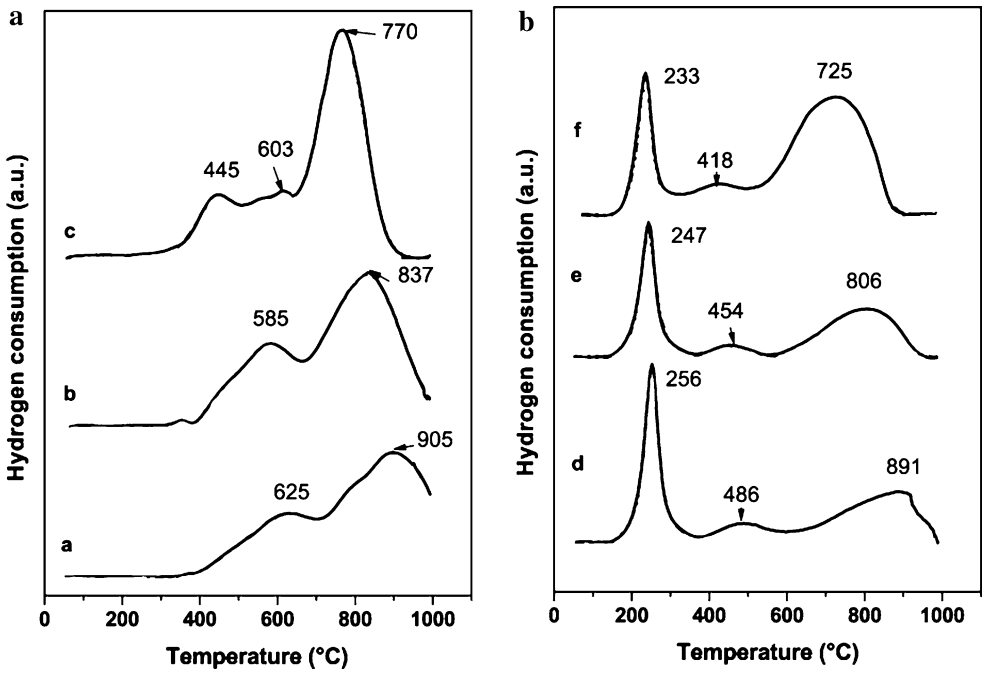

Fig. 1 **a** TPR profiles for the oxide catalysts *a* NiW/Al, *b* NiW/AT10, *c* NiW/AT2, calcined at 400 °C. **b** TPR profiles for the sulfided catalysts *d* NiWS/Al, *e* NiWS/AT10, *f* NiWS/AT2, sulfided at 400 °C

during the TPR experiments (NiW/AT2 > NiW/AT10 > NiW/Al), the largest HDS activity of the NiW/AT2 sulfide catalyst could be linked with the largest amount of WO_3 precursor species.

3.1.3 X-ray Photoelectron Spectroscopy (XPS)

The lower metal–support interaction would result in a greater sulfidation such as shown in the XPS results. The quantitative estimation for the freshly sulfided (at 400 °C) catalysts XPS spectra is displayed in Table 3. The W 4f peak shows two doublets, each one with the $4f_{7/2}$ and $4f_{5/2}$ components (Figure not shown here) coming from the spin–orbit splitting. The relative amount of WS_2 species (W $4f_{7/2}$, 32.5–32.7 eV) and NiWS (Ni $2p_{3/2}$, 853.9 eV) [38] is indicated in parentheses.

Additionally, the Ni $2p_{3/2}$ core level spectra of all the catalysts show a component at a BE of 856.5 eV, which is typical of Ni^{2+} ions interacting strongly with the alumina substrate forming a non-sulfide $NiAl_2O_4$ spinel-like species [39]. The NiW/AT2 catalyst exhibits a lower amount of $NiAl_2O_4$ spinel-like compounds than the other NiW/Al and NiW/AT10 samples. Similarly, the W $4f_{7/2}$ component at higher binding energy (35.9 eV) is clearly due to non-sulfide W–O moieties [39]. The presence of these non-sulfide W species is expected because WO_3 is fully sulfided at temperatures somewhat about 500 °C.

However, some oxidation of the fresh sulfided samples during the sample handling from the catalytic reactor to the XPS chamber can be excluded because nickel sulfide species were not oxidized.

It can be seen that the samples exhibited a similar percent of WS_2 species (~25 %). However, regarding Ni species, the NiW/AT2 catalyst presents a higher percent of sulfur species than the others catalysts to form the NiWS (45 %) phase. Besides, NiW/Al and NiW/AT10 catalysts showed a lower amount of these species, 34 and 19 %, respectively. Considering the results by Reinhoudt et al. [3, 5], one might expect that after sulfidation at 350 °C for 2 h, the sulfidation degree for W and Ni species should be about 21 and 58 %, respectively. To determine the relative abundance of atoms of Ni and W exposed at the surface for different samples the atomic ratios S/(Ni + W), W/(Al + Ti) and Ni/(Al + Ti) were calculated and presented in Table 3. An increase of 86 % in the W amount and a 26 % increase in the Ni amount on the surface can be seen

Table 3 Binding energies (eV) and atomic surface ratios of the NiW/Al and NiW/Al_2O_3–TiO_2 catalysts sulfided at 400 °C

Catalyst	W $4f_{7/2}$	Ni $2p_{3/2}$	S/(Ni + W)	W/(Al + Ti)	Ni/(Al + Ti)
NiW/A1	32.6 (23 %)	853.9 (34 %)	1.20	0.080	0.056
	35.9 (77 %)	856.5 (66 %)			
NiW/AT10	32.5 (23 %)	853.8 (19 %)	0.93	0.108	0.078
	36.0 (77 %)	856.4 (81 %)			
NiW/AT2	32.7 (25 %)	853.9 (45 %)	1.28	0.149	0.071

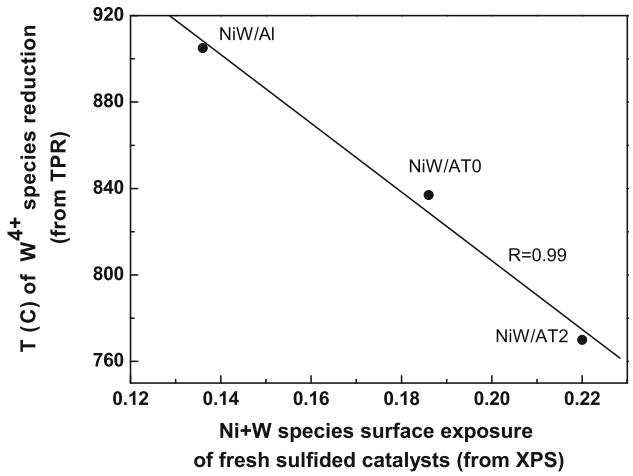

Fig. 2 Correlation between the metal species surface exposure for fresh sulfided catalysts and the reduction temperature needed for formation of metallic W species ($W^{4+} \rightarrow W^0$)

for the NiW/AT2 catalyst with respect to NiW/Al catalyst. This may indicate a higher dispersion by increasing the amount of Ti in the support. Also, it is possible to observe a slight increase in the S/(Ni + W) ratio with the increase of titania in the support, indicating that there is a higher sulfidation of the NiW/AT2 catalyst than the others. This result may be caused by the lower metal–support interaction upon the addition of Ti. Interestingly, it was found a correlation between the metal species surface exposure (from XPS) and the support–metal interaction deduced from temperature maxima when W^{4+} species transformation into metallic W occurred (from TPR). Figure 2 shows the maximum temperature needed for formation of metallic W species ($W^{4+} \rightarrow W^0$) against the metal species surface exposure for fresh sulfided catalysts (from Table 3). As seen in this figure, the NiW/AT2 sample with the largest metal species surface exposure exhibited the lowest support–metal interaction among the studied catalysts.

3.1.4 High Resolution Transmission Electron Microscopy (HRTEM)

The Fig. 3 shows sulfided catalysts micrographs. It is possible to observe the presence of typical WS_2 phase slabs

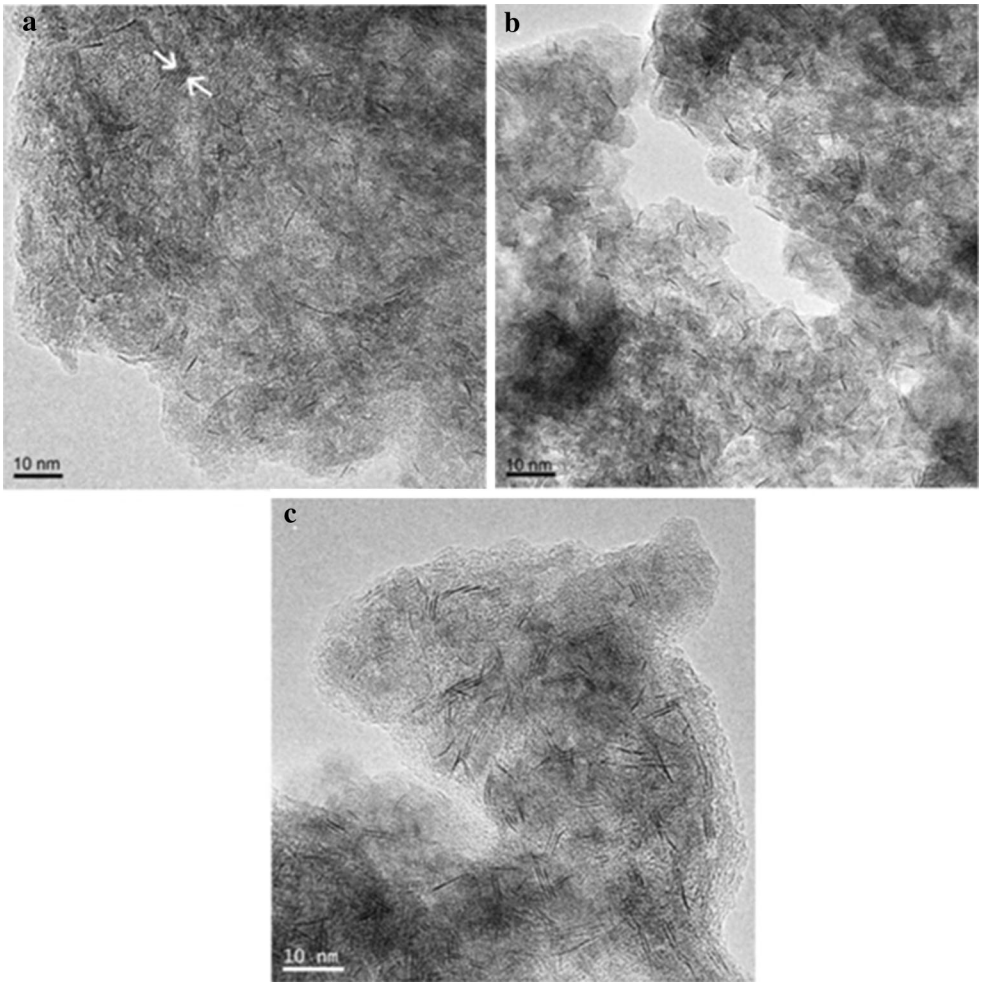

Fig. 3 HRTEM micrograph of the **a** NiW/Al, **b** NiW/AT10, and **c** NiW/AT2 catalyst sulfided at 400 °C

structures, which are dispersed homogeneously on the support and large aggregates of WS_2, were not found. It is can be seen in Fig. 3 that all sulfided samples exhibited mainly parallel oriented to the electron beam direction edge WS_2 slabs. Another orientation as the basal plane of the WS_2 slabs can be identified, however this orientation is less abundant compared to the predominant above. Thus the HRTEM images for all sulfide catalysts showed the presence of WS_2 species corresponding to hexagonal crystal structure and W atoms located in trigonal prismatic coordination sphere. The interplanar gap ($\sim$0.62 nm) is consistent with the basal plane (0 0 2) within WS_2 [39]. The WS_2 slabs length and number distribution are given in Fig. 4.

As seen in Fig. 4a, titania-containing catalysts have a slightly wider crystallite size distribution than the supported on alumina. As a result, the average WS_2 crystal size increased as noted in the following sequence: NiW/Al (2.5 nm) < NiW/AT10 (2.6 nm) < NiW/AT2 (3 nm).

Thus, contrasting with results published by Ramirez et al. [9], both titania-based catalysts showed a slight increase in the crystal size with respect to the titania-free catalyst. Considering the TPR results, this is related to a decrease in the metal–support interaction for supported Al_2O_3–TiO_2 catalyst with respect to NiW/Al. As a consequence of a weaker support–metal interaction, both titania-containing catalysts showed a higher degree of sulfidation than the alumina supported catalyst, as it was displayed in the XPS results (see Table 2). Finally, it can be noted that NiW/AT2 catalyst shows a slight increase in the number of stacked slabs respect to the other two catalysts (2.8 vs 2.5).

3.2 Catalytic Measurements

Figure 5 shows the initial rate of disappearance of the DBT and 4,6-DMDBT molecules for sulfided NiW catalysts at 400 °C.

In general, the AT2 supported catalysts exhibited significantly higher catalytic efficiency in the HDS of DBT and 4,6-DMDBT compared with the other solids. The NiW/AT2 catalyst showed approximately 70 and 60 % higher activity than the equivalent supported on Al_2O_3 for DBT and 4,6-DMDBT respectively.

At 25 % of conversion, the products detected in the HDS of 4,6-DMDBT over all catalysts studied were (Table 4): 3,3′-dimethylbiphenyl (3,3-DMBP), 4,6-dimethyltetrahydrodibenzothiophene (4,6-DMTHDBT), dimethylcyclohexylbenzene (DMCHB) and dimethylbicyclohexyl (DMBCH). Thus, the 4,6-DMDBT undergoes HDS via direct desulfurization (DDS) leading to the formation of 3,3-DMBP compound and via hydrogenation (HYD) giving intermediate 4,6-DMTHDBT, which after sulfur removal through C–S bond scission is converted to DMCHB (a slow reaction) and then to DMBCH. For all catalysts, the 4,6-DMDBT converts mainly via the HYD pathway, as deduced from comparison of the selectivity ratio (k_{HYD}/k_{DDS}) and products yields. However, significant changes in the selectivity between NiW/Al and NiW/AT2 catalysts were not observed (Table 4).

This activity increase was the result of significant changes in the structural and surface properties of the support, favorably influencing support–metal interactions. On one hand, the structural conformation shown by AT2

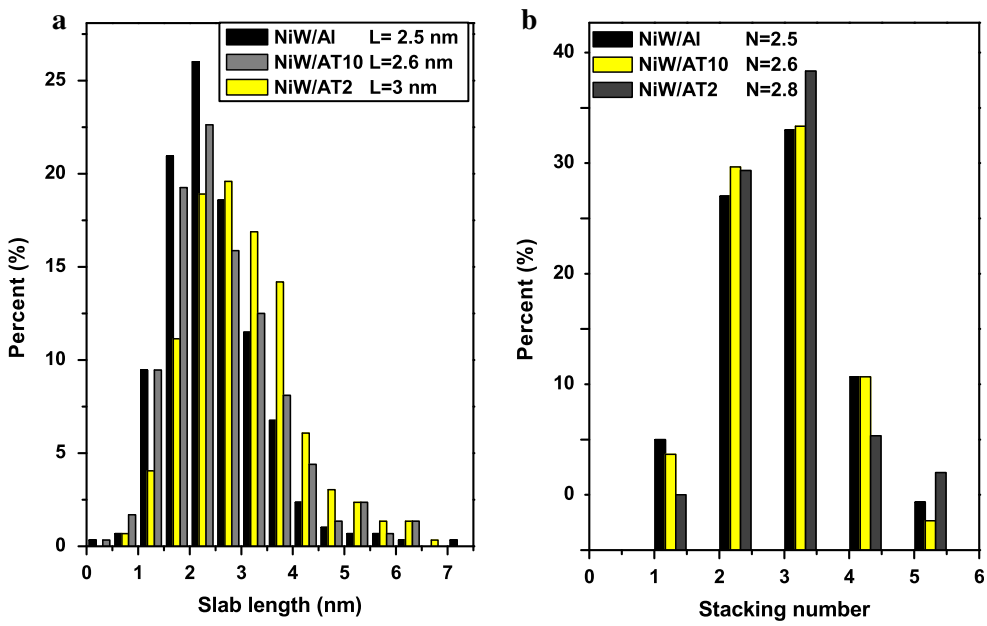

Fig. 4 NiW catalysts crystallites size distribution. *Left* **a** slabs length and *right* **b** stacking number

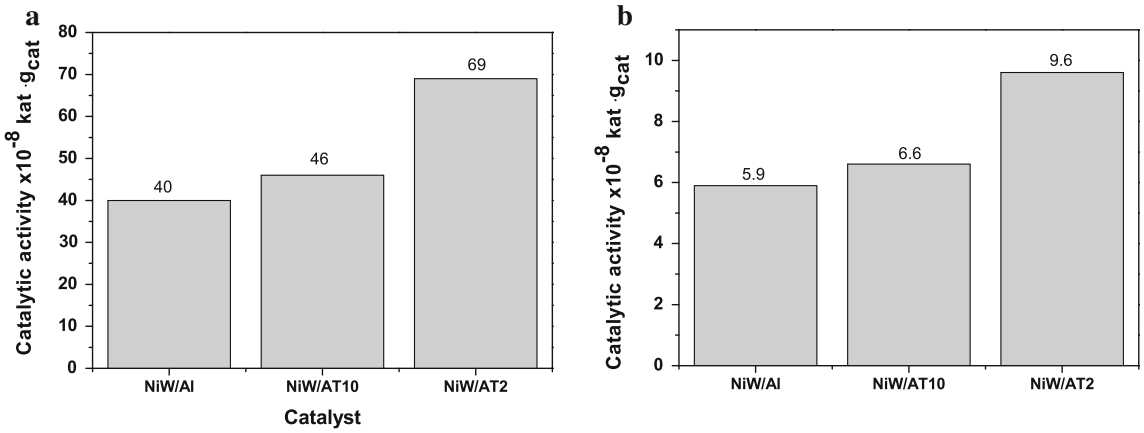

Fig. 5 Catalytic initial activity in the HDS of **a** DBT and **b** 4,6-DMDBT with NiW catalysts supported on Al_2O_3–TiO_2 (17 % W and Ni/(Ni + W) = 0.5)

Table 4 Percentage of selectivity and products yield for the HDS of 4,6-DMDBT at 25 % of conversion

Catalyst	3,3-DMBP (%)	4,6-DMTHDBT (%)	DMCHB (%)	DMBCH (%)	k_{HYD}/k_{DDS}
NiW/Al	8	4	13	0	1.53
NiW/AT2	7	5	12	2	1.52

support [26, 28], induced significant changes in the total acidity of the support (40 % less acidity) and a decrease of the point of zero charge, while AT10 support showed no significant changes from Al_2O_3.

In Fig. 6 an increase in the initial reaction rate is observed, related to a decrease in the amount of strong acid sites, which are lower for the NiW/AT2 catalyst, as determined by NH_3-TPD technique. Due to the fact that Ti^{4+} ions are Lewis acidic sites [40] and alumina alone possesses both Lewis and Brønsted acid sites [41], for all catalysts the nature of strong acid sites should be both Brønsted and Lewis acids (main acidity). In this sense, an increase in Lewis acidity with an increase of Ti content in hybrid HMS-Ti was previously reported [40].

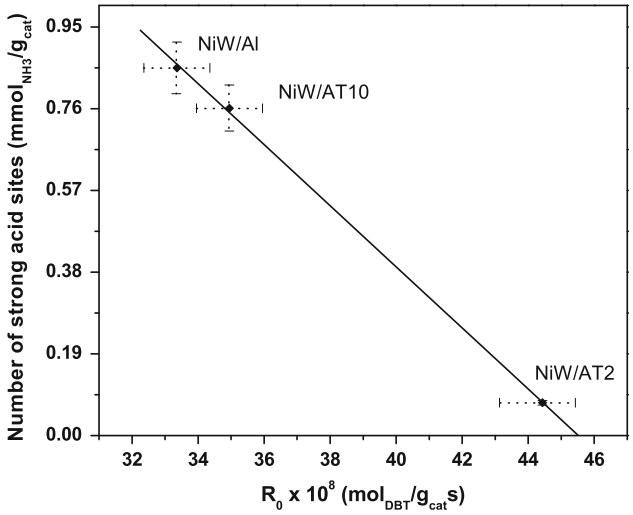

Fig. 6 Influence of strong acid sites on the catalyst activity on the HDS of DBT

The influence of the support (Al_2O_3 against Al_2O_3–TiO_2) on the coking behaviour of sulfided NiW catalysts in HDS reaction was evaluated from the weight change of the coked catalysts during temperature-programmed oxidation by means of TG-DTG technique. Figure 7 presents the TPO/TG-DTG plots of the spent NiW/Al, NiW/AT2 and NiW/AT10 catalysts. The weight loss in the TG profiles, corresponding to the most intense DTG peak centred at 460 °C can be assigned to lose of the sulfur atoms from oxo-sulfide species whereas the second weight loss (DTG peak centred at ~700 °C) is characteristic of coke oxidation [42]. Table 5 compiles the weight loss corresponding to the decomposition of metal sulfide species and oxidation of coke. The weight loss in temperature range 300–600 °C (DTG peak centered at around 460 °C) was observed. This weight loss in this temperature region is commonly described in literature as due to the oxidation of metal sulfide species leading to SO_2 evolution. Interestingly, we found that two catalysts supported on alumina modified with TiO_2 (NiW/AT2 and NiW/AT10) exhibited a lower SO_2 evolution than the catalyst supported on alumina (NiW/Al) indicating the enhanced stability of the metal sulfides or oxo-sulfides species when the support was modified with TiO_2.

On the other hand, different temperature at which oxidation of coke occurs (NiW/AT2 (679 °C) < NiW/AT10

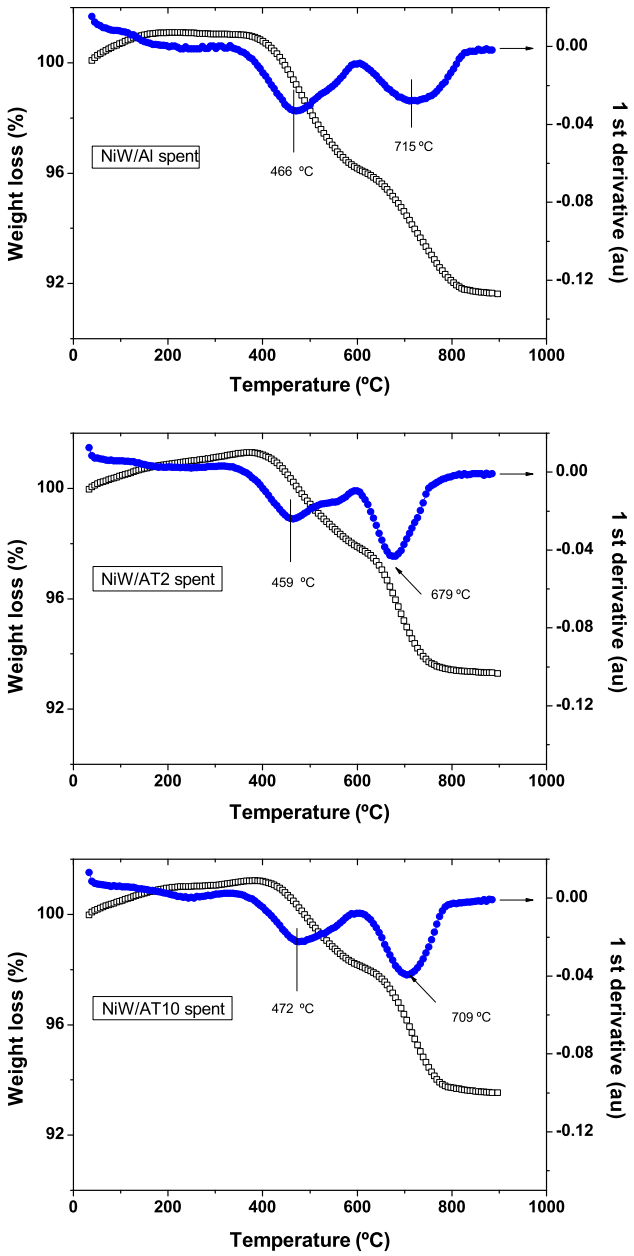

Fig. 7 TPO/DTG plots of the spent NiW/Al, NiW/AT2 and NiW/AT10 catalysts

(709 °C) < NiW/Al (715 °C)) might indicate that more polymerized coke is formed on the NiW/Al sample. However, considering the weight loss corresponding to coke burning (Table 5), one might conclude that similar amount of coke was formed on all binary samples.

The highly disperse Ti^{4+} into alumina network may be taking place within the surface Al^{3+} vacancies and decreasing the strong acid sites and limiting the migration of Ni into the Al_2O_3 matrix [19, 27]. In addition, NiW/AT2 catalyst TPR profiles showed a clear decrease of the reduction temperature of the supported metal species, with

Table 5 Weight loss between 300 and 900 °C for the spent catalysts

Sample	SO_2 evolution		Coke	
	T (°C)	Weight loss (%)	T (°C)	Weight loss (%)
NiW/Al	466	5.6	715	4.1
NiW/AT2	459	3.5	679	4.5
NiW/AT10	472	3.3	709	4.5

As determined by TPO/TG-DTG technique

a significant increase in H_2 consumption related to the reduction of W species. Since the catalyst initial activities (Fig. 5a, b) follows the same trend as the H_2 consumed during the TPR experiments (NiW/AT2 > NiW/AT10 > NiW/Al), the largest HDS activity of the NiW/AT2 sulfide catalyst could be linked with the largest amount of WO_3 species of its oxide precursor.

Regarding this, the Raman spectra of these materials, exposed in Fig. 8, showed that the catalyst supported on the mixed oxide AT2 may possess the smallest fraction of surface W species (O = W: between 950 and 1000 cm^{-1}; and O = W = O: 850–1000 cm^{-1}) with respect to the bulk particle (W = O + O = W = O)/O–W–O, which could indicate the formation of larger WO_X species [30]. Together these results suggest that the AT2 support would favor the availability of the metal oxides, WO_X and NiO_X, due to a weaker metal–support interaction.

We further investigated the support effect on the type of species formed after catalyst sulfidation at 400 °C by performing the XPS analysis. As expected, the observed characteristics of the oxide phase were correlated with the formation of the sulfide phase (Fig. 9). Specifically, the XPS spectra of sulfided NiW/AT2 catalysts showed the

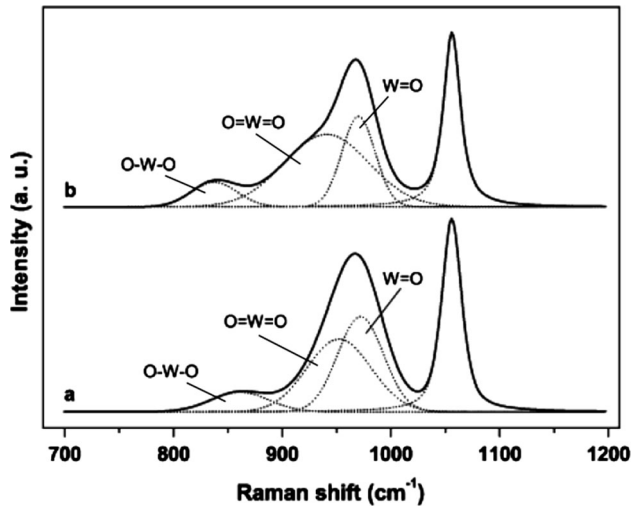

Fig. 8 Raman spectra with Gaussian deconvolution of the catalyst calcined at 400 °C **a** NiW/Al and **b** NiW/AT2

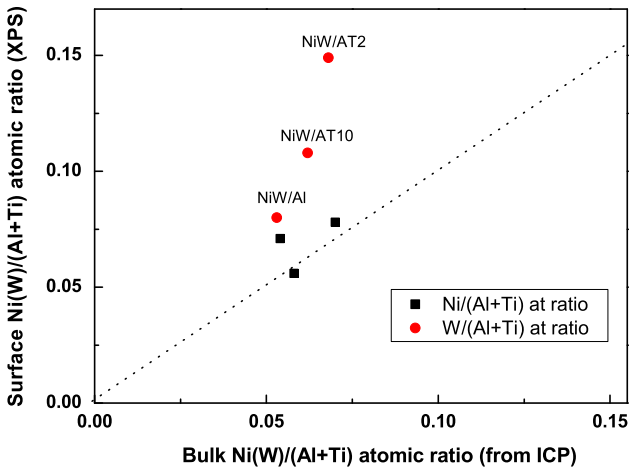

Fig. 9 Surface exposure of Ni and W species (from XPS) for the sulfided catalysts against the bulk Ni(W)/(Al + Ti) atomic ratio of the respective oxide precursors (from chemical analysis)

highest fraction of surface WS_2 and the promoted phase "NiWS". To determine the possible location of Ni and W, in Fig. 9 are plotted the surface Ni(W)/(Al + Ti) atomic ratio of the sulfided samples against the bulk Ni(W)/(Al + Ti) atomic ratio of their respective oxide precursor (from chemical analysis). For all samples, the Ni species was found to be more homogeneously distributed than W ones. Interestingly, the incorporation of Ti on the alumina forced location of the W species on the outer catalyst surface. After sulfidation, the NiW/AT2 exhibits a larger amount of W species on the outer catalyst surface than its NiW/AT10 counterpart.

The TPR profiles analysis of the sulfided catalysts confirmed these findings regarding the WO_X and NiO_X availability to be sulfided when supported on AT2. In particular, the sulfided NiW/AT2 catalyst showed higher amount of sulfur species as compared with the other catalysts. Moreover, the increased H_2 consumption was relative to labile sulfur reduction, which was related to the formation of coordinated unsaturated sites (CUS) on the metals or anionic sulfur vacancies. For the sulfided catalyst, HRTEM characterization showed that AT2 support induced an increase in the WS_2 slab size and stacking, which may have its origin in the formation of larger WO_X particles during calcination linked with a lower W–support interaction. According to the above, using AT2 as catalyst support may lead to an easier sulfidation of the W species and increases the availability of the promoter metal, compared to the Al_2O_3 supported catalyst, this was reflected in a significant increase in catalytic activity in the HDS of DBT and 4,6-DMDBT. The Fig. 10 shows a schematic representation of the described above.

4 Conclusions

The AT2 support increased the formation of the NiWS active phase, reflected in a significant increase in the catalytic activity of HDS of DBT and 4,6-DMBDT. The incorporation of Ti in the Al_2O_3 matrix (Al/Ti = 2) by the sol–gel method a decreasing in a Al^{3+} vacancies was originated, which have affinity to surface Ni^{2+}, this led to a higher number of NiO_X species formation, which are the precursor of promoted WS_2 phase. The increase in the NiO_X species results in a higher availability of promoter metal to the set of edges of WS_2 platelets during sulfidation, increasing the fraction of active sites, NiWS, promoting activity in hydrodesulfurization.

Acknowledgments Authors appreciate financial support from Consejo Nacional de Ciencia y Tecnología (CONACyT) and Fondo de Cooperacion Internacional en Ciencia y Tecnología (FONCICyT) for their support in the project 96164. We express our gratitude to the research groups from the Universidad Autonoma Metropolitana – Iztapalapa (Mexico), the Universidad Autónoma del Estado de Hidalgo (Mexico), the Instituto de Catálisis y Petroleoquímica del CSIC (Madrid, Spain) and Institut de Recherches sur la Catalyse et l'environement de Lyon (France) for their efforts, professionalism and attention to this work.

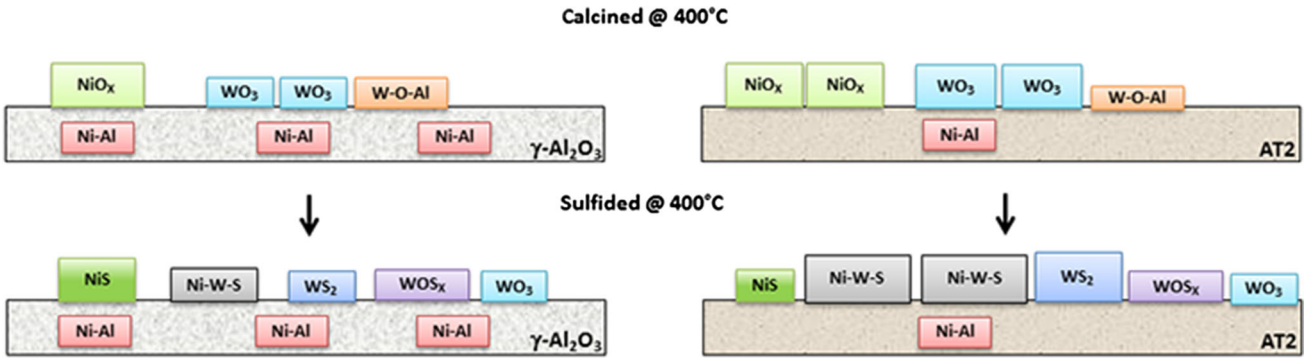

Fig. 10 Schematic representation of the supported W species on Al_2O_3 and AT2 mixed oxide

References

1. Stanislaus A, Marafi A, Rana MS (2000) Catal Today 153:1–68
2. Robinson WRAM, van Veen JAR, de Beer VHJ, van Santen RA (1999) Fuel Process Technol 61:103–116
3. Reinhoudt HR, Troost R, van Langeveld AD, van Veen JAR, Sie ST, Moulijn JA (2001) J Catal 203:509–515
4. Kameoka T, Yanase H, Nishijima A (1995) Appl Catal A 123:217–228
5. Reinhoudt HR, van Langeveld AD, Mariscal R, de Beer VHJ, van Veen JAR, Sie ST, Moulijn JA (1997) Stud Surf Sci Catal 106:228–263
6. Breysse M, Afanasiev P, Geantet C, Vrinat M (2003) Catal Today 86:5–16
7. Hensen EJM, van der Meer Y, van Veen JAR, Niemantsverdriet JW (2007) Appl Catal A 322:16–32
8. Breysse M, Bachelier J, Bonnelle JP, Cattenot M, Cornet D, Décamp T, Duchet JC, Durand R, Engelhard P, Frety R, Gachet C, Geneste P, Grimblot J, Gueguen C, Kasztelan S, Lacroix M, Lavalley JC, Leclercq C, Moreau C, De Mourgues L, Olivé JL, Payen E, Portefaix JL, Toulhoat H, Vrinat M (1987) Bull Soc Chim Belg 96:829–844
9. Ramírez J, Gutíerrez-Alejandre A (1998) Catal Today 43:123–133
10. Vissenberg MJ, van der Meer Y, Hensen JM, de Beer VHJ, van der Kraan AM, van Santen RA, van Veen JAR (2001) J Catal 198:151–163
11. Toulhoat H, Raybaud P (2013) Catalysis by transition metal sulfides. Editions Technip, Paris
12. Saih Y, Nagata M, Funamoto T, Masuyama Y, Segawa K (2005) Appl Catal A 295:11–22
13. Guevara-Lara A, Bacaud R, Vrinat M (2007) Appl Catal A 328:99–108
14. Song H, Dai M, Guo YT, Zhang YJ (2012) Fuel Process Technol 96:228–236
15. Pophal C, Kamdea F, Hoshino K, Yoshinaka S, Segawa K, Kameda F, Hoshino K, Yoshinaka S, Segawa K (1997) Catal Today 39:21–32
16. Srinivas BN, Maity SK, Prasad VVDN, Rana MS, Kumar M, Kumar M, Prasada Rao TSR (1998) Stud Surf Sci Catal 113:497–506
17. Maity SK, Ancheyta J, Soberanis L, Alonso F, Llanos ME (2003) Appl Catal A 244:141–153
18. Bej SK, Maity SK, Turanga UT (2004) Energy Fuels 18:1227–1237
19. Escobar J, de los Reyes JA, Viveros T (2003) Appl Catal A 253:151–163
20. Duan A, Li R, Jiang G, Gao J, Zhao Z, Wan G, Zhang D, Huang W, Chung K (2009) Catal Today 140:187–191
21. Maity SK, Ancheyta J, Rana MS, Rayo P (2006) Energy Fuels 20:427–431
22. Ramírez J, Gutiérrez-Alejandre A (1997) J Catal 170:108–122
23. Gutiérrez-Alejandre A, Ramírez J, Jiménez-del Val I, Peñuelas-Galaz M, Sánchez-Neri P, Torres-Mancera P (2005) Catal Today 107–108:879–884
24. Ramírez J, Macías G, Cedeño L, Gutiérrez-Alejandre A, Cuevas R, Castillo P (2004) Catal Today 98:19–30
25. Cruz-Perez AE, Guevara-Lara A, Morales-Cerón JP, Álvarez-Hernández A, de los Reyes JA, Massin L, Geantet C, Vrinat M (2011) Catal Today 172:203–208
26. Escobar J, de los Reyes JA, Viveros T (2000) Ind Eng Chem Res 39:666–672
27. Montoya JA, del Ángel P, Viveros T (2001) J Mater Chem 11:944–950
28. Núñez S, Escobar J, Vázquez A, Vázquez A, de los Reyes JA, Hernández-Barrera M (2011) Mater Chem Phys 126:237–247
29. Navarro R, Pawelec B, Fierro JLG, Vasudevan PT, Cambra JF, Arias PL (1996) Appl Catal A 137:269–286
30. Díaz de León JN, Picquart M, Villarroel M, Vrinat M, Gil Llambias FJ, Murrieta F, de los Reyes JA (2010) J Mol Catal A 323:1–6
31. Blanchard P, Lamonier C, Griboval A, Payen E (2007) Appl Catal A 322:33–45
32. Prada Silvy R, López F, Romero Y, Reyes E, León V, Galiasso R (1995) Stud Surf Sci Catal 91:281–290
33. Koutsospyros A, Braida W, Christodoulatos C, Dermatas D, Strigul N (2006) J Hazard Mater 136:1–19
34. Scheffer B, Molhoek P, Moulijn JA (1989) Appl Catal 46:11–30
35. Zuo D, Vrinat M, Nie H, Maugé F, Shi Y, Lacroix M, Li D (2004) Catal Today 93–95:751–760
36. Mangnus PJ, Bos A, Moulijn JA (1994) J Catal 146:437–448
37. Scheffer B, Mangnus PJ, Moulijn JA (1990) J Catal 121:18–30
38. Grimblot J, Gengembre L, Huysser AD (1990) J Electron Spectrosc Relat Phenom 52:485–509
39. Cruz J, Avalos-Borja M, López Cordero R, Bañales MA, Fierro JLG, Palacios JM, López Agudo A (2002) Appl Catal A 224:97–110
40. Zepeda TA, Pawelec B, Fierro JLG, Halachev T (2006) J Catal 242:254–269
41. Guillaume D, Gautier S, Despujol I, Alario F, Beccat P (1997) Catal Lett 43:213–218
42. Soares RW, Menezes VJ, Fonseca VA, Dweck J (1997) J Therm Anal Calorim 49:657–661